Generating and Analyzing Synthetic Finger Vein Images

Fieke Hillerström[1,2], Ajay Kumar[1], Raymond Veldhuis[2]

[1]Department of Computing
The Hong Kong Polytechnic University
[2]University of Twente, The Netherlands
Email: csfhhillerstrom@comp.polyu.edu.hk, csajaykr@comp.polyu.edu.hk,
R.N.J.Veldhuis@utwente.nl

Abstract: The finger-vein biometric offers a higher degree of security, personal privacy and strong anti-spoofing capabilities than most other biometric modalities employed today. Emerging privacy concerns with the database acquisition and lack of availability of large scale finger-vein databases have posed challenges in exploring this technology for large scale applications. This paper details the *first* attempt to synthesize finger-vein images and presents analysis of synthesized images for the biometrics authentication. We generate a database of 50,000 finger-vein images, corresponding to 5000 different subjects, with 10 different synthesized finger-vein images from each of the subject. We use tractable probability models to compare synthesized finger-vein images with the *real* finger-vein images for their image variability. This paper also presents matching accuracy using the synthesized finger-vein database from 5000 different subjects, using 225,000 genuine and 1249,750,000 impostor matching scores, which suggests significant promises from finger-vein biometric modality for the large scale biometrics applications.

1 Introduction

Biometric identification using finger-vein patterns typically matches the profile of subcutaneous finger-vein network. The finger-vein biometric is not visible under normal illumination conditions which makes it very difficult to covertly acquire and extremely difficult to alter their integrity. Therefore finger-vein biometrics offers high degree of privacy, anonymity, security and anti-spoofing capability over other popular biometrics like face, iris or even fingerprint. Several databases of finger-vein images have recently been introduced [KZ12, YLS11, TV13, ZLL+13, MASR14]. However, these databases are relatively smaller than those available for face or iris and involve a small number of subjects for imaging (see table 2). Therefore it is impossible to subject the developed identification algorithms to extensive testing. The acquisition of large scale biometric databases is expensive, inconvenient for the subjects, and comes with the privacy concerns related with biometrics. In order to address some of these problems, several synthetic biometric databases have been developed [Cap04, ZSC07, WHST08]. However, finger-vein image synthesis had not yet attracted the attention of researchers.

In this paper we develop a finger-vein image synthesis model, based on vein pattern growth from nodes to patterns, which incorporates realistic imaging variations to

synthesize finger-vein images for biometrics. The anatomy of the finger-veins is firstly analyzed (section 3) and the influence of finger-vein acquisition methods is then introduced (section 4). These formulations are used as a basis for the generation of synthetic finger-vein images (section 5). The performance of a developed synthetic finger-vein image database is analyzed (section 6), using tractable probability models and also the actual matching performance.

Table 1: Summary of prior work on biometric image synthesis for different modalities

Modality	Reference	Approach	Database
Iris	[7]	Generation of synthetic fibers and adding top layers	200 individuals, 2 iris classes per individual, 6 iris images per class
Fingerprint	[6]	Generation of directional map and ridge pattern, combined with a density map	Adjustable up to 100000 fingers with each up to 100 samples
Face	[11]	Forming linear combinations of prototypes derived from real faces	Not available
Palmprint	[8]	Patch-based sampling on extracted principle lines	300 classes with each 20 images. Total images: 6000
Finger-Vein	*This Paper*	Random vein pattern growth combined with imaging variability models	**5000** subjects with each 10 finger-vein images, Total images: **50,000**

Table 2: Summary of the finger-vein image databases developed in the references

| Database	Reference	Size	Sessions	Public
The Hong Kong Polytechnic University	[1]	6264 images from 156 subjects, 2 fingers per subject	2	Yes
SDUMLA-HMT	[2]	3816 images, 6 fingers per subjects	1	Yes
University of Twente	[3]	1440 images of 60 subjects	2	No
CFVD	[4]	1345 images of 13 subjects, 130 different fingers	2	No
FV-USM	[5]	5904 images of 123 subjects, 492 different finger classes	2	Yes

2 Related Prior Work

There has been an increasing interest to explore vascular patterns for biometrics identification [KP09], [KZ12]. Several commercial systems have already been introduced and available for commercial usage. Earlier efforts to match finger-vein patterns using repeated line tracking approach is described in [MNM04]. Yang *et al*. [YSY10] investigated the finger-vein authentication using a bank of Gabor filters. Several publications illustrate local binary pattern based matching of finger-vein features [RSS11, LLP09]. One of the most comprehensive works on finger-vein identification, with comparison of multiple finger vein matchers on relatively larger database, appears in [KZ12]. This paper also proposes to enhance finger-vein identification using simultaneously extracted fingerprint images.

Another approach to improve finger-vein recognition accuracy is to perform restoration of finger-vein images degraded by the light scattering in the finger skin. Such an approach is described in [YSY12] and uses a biologically motivated optical model. Lee and Park [LP11] use an image restoration model that can account for optical blur and skin scattering, to improve the finger-vein matching accuracy.

Synthesis of biometric images enables modeling of vital anatomical evidences underlying the respective biometric images and noise obscuring the recovery of underlying features. The image synthesis also enables development of large scale biometrics databases for the performance evaluation and improvement in the real systems. Another use of synthesized biometrics database lies in detecting and evaluating integrity of a given biometrics system. There have been several promising efforts to

synthesize biometrics image databases for other popular biometric modalities. Table 1 summarizes such related prior work and also underlines our work in this paper.
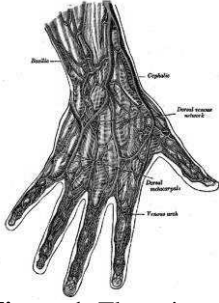
Figure 1: The veins on dorsum of the hand [17].
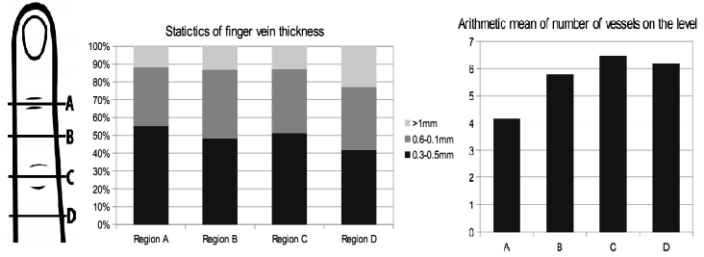
Figure 2: Typical statistics of blood veins in human fingers.

3 Anatomy of Finger-Veins

The veins in the fingers can be divided into two sets, the superficial veins and the deep veins. The deep veins lay usually alongside the arteries, where the superficial veins are closer to the surface of the body [Gra18]. The superficial veins of the hand contain the dorsal digital veins and the palmar digital veins, which pass along the sides of the fingers and contain a venous network in between [Gra18] (see figure 1). Loda states that the veins in the finger are located almost exclusively at the dorsal side of the finger [Lod99]. From the nail, small veins meet at the distal interphalangeal joint where they form one or two small central veins, with a diameter of approximately 0.5 mm [Lod99]. The veins become more prominent and numerous at the proximal interphalangeal level, where they form anastomotic arches. Sukop *et al*. [SND+07] found that the three-phalanx fingers contain the same typical statistics about the dorsal venous systems (figure 2). There are two veins at both the radial and ulnar side of the proximal phalanx with a diameter over 1 mm, leading to the hand palm. These two veins form an arch above the proximal phalanx [SND+07].

4 Imaging Variation in Finger-Vein Images

The finger-vein imaging typically uses near infrared (NIR) spectroscopy, with a wavelength between 700nm to 1400nm [XS08]. The veins become visible, because of the hemoglobin in the blood plasma. At 760 nm light-absorption is almost only performed by de-oxidized hemoglobin and not by oxidized hemoglobin [CC+07]. When a suitable wavelength is chosen, the arteries, which contain mostly HbO, will not be visible in the finger-vein image. The NIR-scanning device cannot penetrate deep into the skin and therefore the deep veins are not captured in the images [CC+07]. The interphalangeal joints result in a higher light penetration through the finger, because the joint is filled with fluid, which has a lower density than bones [YS12]. This is the key reason for the illumination variation commonly observed in finger-vein images.

While acquiring the finger-vein patterns, the images are expected to be degraded, due to scattering and optical blur. Such depth-of-field blur of the camera can be modeled using Gaussian blur [KP07], whose parameters can be experimentally estimated. Such point spread function (PSF) can be defined as

$$h(x,y) = \frac{1}{2\pi\sigma^2} e^{-\frac{x^2+y^2}{2\sigma^2}}$$ (1)

with as parameters $\sigma = kR$ and (x,y) are the spatial indices. k is a parameter determined by the camera properties. R represents the radius of the blur, defined as;
$R = \frac{Ds}{2}\left(\frac{1}{f} - \frac{1}{u} - \frac{1}{s}\right)$ in which D is the diameter of the lens aperture, s the distance between the lens and the image plain, f the focal distance of the camera and u the distance between the lens and the object, which will vary for every finger-vein image.

The finger-vein images are also expected to be degraded due to skin scattering, which can be modeled by a model which includes the absorption and scattering coefficients of the skin and the thickness of the skin [LP11]. At a wavelength of 850 nm the absorption and scattering coefficients of the finger skin are 0.005 and 0.61 mm^{-1} respectively and that the thickness of the finger skin is about 3-4 mm [LP11]. The PSF can be defined as

$$P_s(\rho) = \frac{3P_I}{(4\pi)^2}\left((\mu_s' + \mu_a) + \left(\kappa_d + \frac{1}{\sqrt{\rho^2 + d^2}}\right)\frac{d}{\sqrt{\rho^2 + d^2}}\right) * \frac{e^{-\kappa_d\sqrt{\rho^2+d^2}}}{\sqrt{\rho^2 + d^2}}$$ (2)

with P_I the total power of illumination at a point in the vein region, d the depth of a point from the skin surface, ρ the distance perpendicular to the direction of d. κ is defined as $\kappa_d = 3\mu_a(\mu_s' + \mu_a)$. μ_a is the absorption coefficient of the skin and μ_s' the reduced scattering coefficient.

These two PSFs often degrade the quality of finger-vein images. The NIR-illumination from the source is absorbed by the human tissues, which mainly consists of the skin, bones and vessels. The transmitted light (I_{tr}) after attenuation can be estimated as follows:

$$I_{tr} = I_0 e^{-\mu D}$$ (3)

where I_0 represents the finger-vein image without any degradation, D is the depth of the object and μ is the transport attenuation coefficient [YSY12].
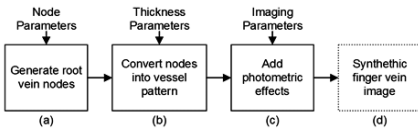

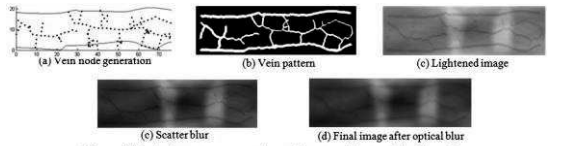Figure 3: Block diagram of key steps for synthesizing finger vein images.

Figure 4: Typical output corresponding to key steps illustrated in Figure 3.

5 Synthesizing Finger-Vein Images

The proposed method for generating synthetic finger-vein images can be divided into three main parts (see figure 3). Firstly the root vein nodes are generated, based on several node parameters. These root vein nodes are different for different fingers, but are assumed to be stable for images from the same finger, since they represent the anatomy of the finger. The root vein nodes are used to grow the thickened vein patterns for the

synthesized image. Finally the grown vein patterns are used to transform into acquired finger-vein images by incorporating the absorption and scattering of skin and blood (see figure 4). Each of these three key steps is described in the following three subsections.
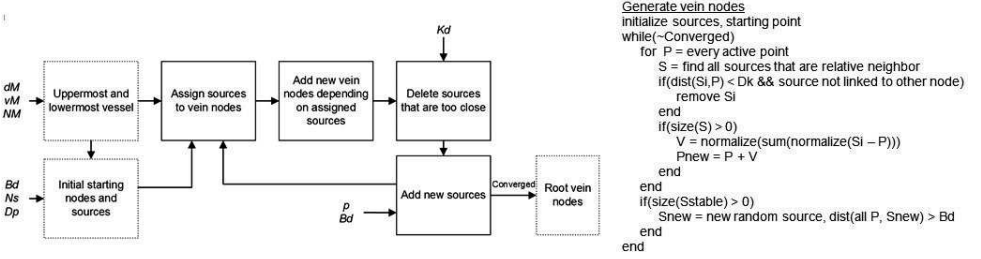

Figure 5: Block diagram and the pseudocode of the key steps for the vein node generation.

5.1 Vein Node Generation

The root finger-vein nodes are generated, using a *grow* method, inspired by the generation of leaf venation patterns proposed in reference [RFL+05]. This model makes use of sources, which influence the direction in which new vessel nodes will be *grown*. An iterative loop is used, to *grow* the veins towards the sources, until the algorithm has converged (see figure 5). During this iterative process new sources are added, which should be further than a *birth distance* B_d from the other sources and veins. A source is removed when a vein reaches that source in the *kill distance* K_d.

The generation of vein nodes largely depends on the sources in the neighborhood. Sources are linked to vein nodes, if they are relative neighbors of each other. For every source linked to a vein node, the normalized vector between them is calculated and these vectors are added up. A new vein node is grown in the resulting direction of this vector. The source should be remained until all nodes growing to the source are in the killing distance of that source.

In our approach the generation of vein nodes begins with two[1] key vessels, on which some stable sources are chosen. Around and between these main vessels, random sources are placed. The growing of new vein nodes will continue until all sources are deleted, or until the sources do not result in new nodes anymore. After all the stable sources are removed, no more new sources will be placed. The finger is divided in three parts based on the locations of the phalanges and according to the statistics observed in [BK10]. Depending on the different part of the finger, the statistics of the source placement differs (see table 3). We select randomly located starting points, to begin the vein generation process.

In order to reduce the computational requirements, we incorporate active vein nodes in our model. When a vein node was not linked to any of the sources for two times, the node becomes inactive. Inactive nodes will not be processed anymore. When a new source is added, all the vein nodes in a certain distance are made active again, to make it possible to grow new nodes towards those newly placed sources.

---

[1] At least two, as indicated from anatomical studies in [SND+07]

| Parameter	Values
Length of the proximal phalanx	39.78 ± 4.94 mm [25]
Length of the medial phalanx	22.38 ± 2.51 mm [25]
Length of the distal phalanx	15.82 ± 2.26 mm [25]
Soft tissues of tip of distal phalanx	3.84 ± 0.59 mm [25]
Distance between source and vein node, in which source will be removed (Kd)	Uniform between 1 and 2
Distance needed for generating a new source in the proximal phalanx (Bdp)	Uniform between 4 and 7
Distance needed for generating a new source in the middle phalanx (Bdm)	Uniform between 4 and 6
Distance needed for generating a new source in the distal phalanx (Bdd)	Uniform between 4 and 5
Distance needed for generating a new source at the edges of the finger (Bde)	Uniform between 2 and 5
Distance needed between the starting points (Bdz)	Uniform between 3 and 10
Distance for which endpoints of lines are added as sources of other vein nodes	Uniform between 5 and 12
Density of generated sources in distal phalanx (Dpd)	Uniform between $\frac{1}{200}$ and $\frac{1}{130}$
Density of generated sources in middle phalanx (Dpm)	Uniform between $\frac{1}{210}$ and $\frac{1}{135}$
Density of generated sources in proximal phalanx (Dpp)	Uniform between $\frac{1}{220}$ and $\frac{1}{140}$
Amount of stable sources in proximal phalanx (Nsp)	3 - 5
Amount of stable sources in middle phalanx (Nsm)	3 - 5
Amount of stable sources in top phalanx (Nst)	2 - 3
Amount of stable sources on the edges of the finger (Nse)	2 - 3
Amount of starting vein nodes (Nsz)	2 - 3
Change that a new source point is generated (p)	Uniform between 0.3 and 0.5
Stepsize between two new nodes	2
Finger width	20 mm
Average distance from main vessels from edge (dM)	Uniform between 1.5 and 5.5
Variance in distance from main vessel from edge (vM)	Uniform between 1 and 2
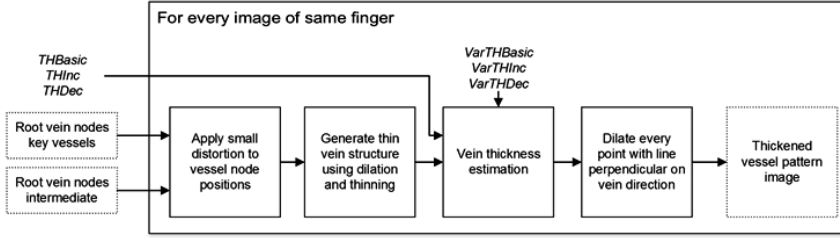
Figure 6: Block diagram of the key steps used to convert the vein nodes into a vein pattern.

5.2 Vein Pattern Generation

Once the desired vein nodes have been generated, these nodes are connected into a thickened pattern that characterizes a vascular network (see figure 6). For every image from the same subject and same finger, a small distortion is added to the positions of the vein nodes, by randomly shifting the basic vein pixels a few pixels. The main vein points and the other vein points are connected to each other separately, using dilation and thinning.

The thickness of the veins is computed, using random basic parameters with small fluctuations for genuine or intra-class images (see table 4). The key uppermost and lowermost vessels are firstly thickened and this process starts from the top (nail end) of the fingers. For every vessel point a small amount of thickness is added. The branches are processed, starting with the veins that branches out of the key vessels (see figure 7). Reference [RFL+05] use Murray's law to calculate the thickness of the branched leaf veins, using $r_{parent}^3 = \sum_1^n r_{child_n}^3$, where r_{parent} represents the thickness of the vein before branching and r_{child} is the thickness of the veins that branches out of the parent vein. This step is incorporated likewise, with the simplification that every child gets the same thickness, $r_{child}^3 = \frac{r_{parent}^3}{N_{child}}$. For every new vein point, the thickness is decreased by small amount/pixels. Veins that are between two branchpoints of a different thickness are assigned the average thickness of both branchpoints. After the thickness is computed for

every vein point, the thinned vein pattern is converted into a thicken image using dilation with a perpendicular line onto the vein direction.
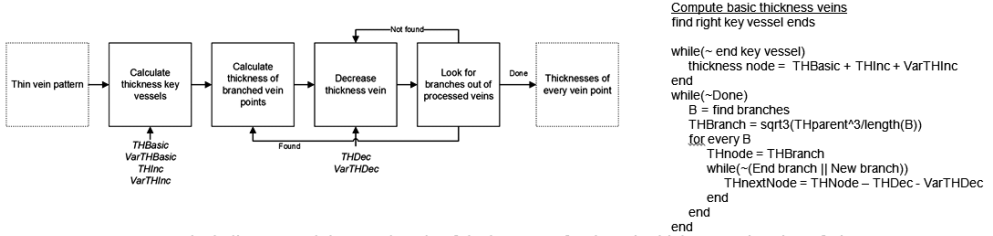

Compute basic thickness veins
find right key vessel ends

while(~ end key vessel)
    thickness node = THBasic + THInc + VarTHInc
end
while(~Done)
  B = find branches
  THBranch = sqrt3(THparent^3/length(B))
  for every B
    THnode = THBranch
    while(~(End branch || New branch))
      THnextNode = THNode – THDec - VarTHDec
    end
  end
end

Figure 7: Block diagram and the pseudocode of the key steps for the vein thickness estimation of Figure 6.

Table 4: Details on the parameters used for the conversion into vessel patterns.

For generating images of different subjects	
Parameter	Values
Width of the dilation structure	15
Minimum thickness of the main vessel (THBasic)	Uniform between 7.5 and 9.4
Thickness increasing for main vessel (THInc)	Uniform between 0.006 and 0.01 – THBasic / 2000
Thickness decreasing for branches (THDec)	Uniform between 0.001 and 0.002 * THBasic
For generating images of same subjects	
Parameter	Values
Variation in minimum thickness of main vessel (VarTHBasic)	Uniform between -2 and 2
Variation in increasing factor for images of same subjects (VarTHInc)	Uniform between -0.006 and 0.006
Variation in decreasing factor for images of same subjects (VarTHDec)	Uniform between -0.0005 and 0.0005 * THBasic /2
Variation in the place of the vessel nodes	4
Variation in the place of the nodes of the main vessels	2

5.3 Finger-Vein Image Generation

The expected influence due to the illumination and the imaging setup are incorporated in the vein pattern images generated (figure 8) from previous section (figure 6). The basic vein patterns generated from the steps in figure 7 are firstly band pass filtered using a Gabor filter, to accentuate different part of the vein patterns. The filter is used for one orientation, with a small variation for every different image of the same subject. The 10 percent lowest outcome values of the Gabor filtering, will be attenuated by a predefined factor (fixed as 4 in our experiments). The illumination effects and variations are modeled using equations (1), (2) and (3). The effect of the depth of the tissues in the finger is varied for every subject and this variation is kept smaller for intra-class images. The bones of the fingers are modeled, using an elliptic function and have a thickness of about 1 cm. The interphalangeal joints are mimicked as two regions of 1.5 - 2 cm, in which the bone thickness is expected to be smaller, according to the observations made in [YS12]. Random points are generated in these areas, which are dilated and the convex hull of these dilated points is estimated. This convex hull is used as area to mimic the
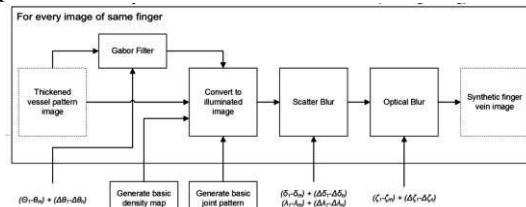

Figure 8: The block diagram for the key steps in the process employed to convert the vein *patterns* into finger-vein images corresponding to near-infrared imaging in the developed synthetic database.

interphalangeal joint. For every image generated from the same subject this joint area is marginally adjusted, using the dilation and erosion with different structuring elements.

In order to incorporate the overall near-infrared illumination (back-lightening) and variability in this illumination from the interphalangeal joints areas, Perlin noise is used. Perlin noise can be used to create coherent noise over space [Per]. Perlin noise with large variety is used to create a more skin like structure and Perlin noise with low variety mimics the overall changes in the light transmission. The parameters incorporated in our synthesis model are provided in table 5.
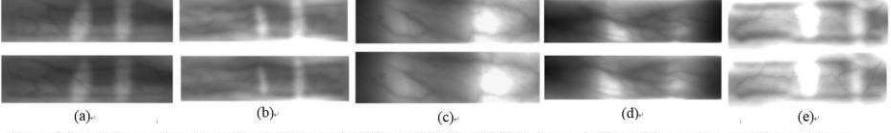

Figure 9: Sample images from the synthesized finger-vein databse in (a), (b) and (e). The images in (c) and (d) are real images from real finger-vein database in [KZ12].

Table 5: Details on the parameters used for the modeling of synthetic finger-vein images.

Generating images from different subjects	
Parameter	Values
Skin thickness	Uniform between 1.5 and 3.5 mm
Range of the basic density map	Values between 0.72 and 1.32
Factor in which bone thickness at joints decreases	Between 0.805 and 0.986
Light absorption of the vessels	40 * skinThickness
Light absorption of skin used in lightening image	200
Light absorption of bones used in lightening image	30
Basic orientation of the Gabor filter (θ_1 - θ_m)	Uniform between $\frac{\pi}{5}$ and $\frac{4\pi}{5}$
Frequency of the Gabor filter	0.08
Size of the Gabor filter	19
Basic depth of the vessels (δ_1 - δ_m)	Uniform between 7 and 15 mm
Basic depth of the tissue (λ_1 - λ_m)	Uniform between 3 and 5 mm
Absorption coefficient of skin used in scatter blur	0.005 / mm
Scattering coefficient of skin used in scatter blur	0.61 / mm
Camera parameter k for optical blur	$\frac{1}{7}\sqrt{3}$
Distance between lens and image plane (ζ_1 - ζ_m)	3.06524 mm
Diameter of lens aperture	6 mm
Basic distance between lens and finger	Uniform between 4 and 6 mm
Focal length of camera	2.753 mm
Width of the joint regions	Uniform between 1.5 and 2 mm
Generating images from same subjects	
Parameter	Values
Dilation and erosion width for adjusting joint regions	Uniform between 8 and 10
Dilation and erosion structures	Diamond, disk or square
Range of Perlin noise to adjust the joint regions	Between 0.7 and 1.3
Variation of orientation of Gabor filter ($\Delta\theta_1$ - $\Delta\theta_n$)	Uniform between -0.1 and 0.1
Multiplication factor of the basic density map	Uniform between 0.99 and 1.01
Variation in the depth of the vessels ($\Delta\delta_1$ - $\Delta\delta_n$)	Uniform between -3 and 3
Variation in the depth of the tissues ($\Delta\lambda_1$ - $\Delta\lambda_n$)	Uniform between -0.25 and 0.25
Variation in the distance between lens and finger ($\Delta\zeta_1$ - $\Delta\zeta_n$)	Uniform between -0.5 and 0.5 mm
Thickness of the vessels	Uniform between 2 and 3 mm

6 Experiments and Results

6.1 Database Generation

We evaluated the proposed approach to synthesize the finger-vein images by generating a large database of 50,000 finger-vein images corresponding to 5000 different subjects. Some of the sample images from the proposed approach are reproduced in figure 9. This figure also includes image samples from the real finger-vein database acquired in [KZ12]. It can be ascertained from the visual inspection that the quality of synthesized finger-vein images is quite similar to those acquired from the real finger-vein imaging setup. The images in figure 10 illustrates typical intra-class and inter-class variations in the synthesized finger-vein images.

(a) Intra-Class (Same Subject)   (b) Inter-Class (Different Subject)
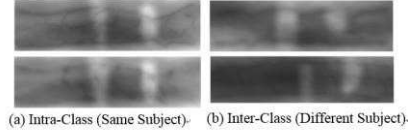
Figure 10: Sample images to illustrate inter-class similarity and intra-class variability.

6.2 Similarity Analysis between Synthesized and Real Images

In order to ascertain distinguishability of synthesized vein images with those acquired from real imaging setup, we model their lower-order probability densities of pixel values in the respective images using Bessel K form [GS01, Sri02]. Grenander and Srivastava [GS01] show that these Bessel K forms can be represented by two parameters: a shape parameter p, $p > 0$ and a scale parameter c, $c > 0$. The image level comparison can be performed by comparing the Bessel K forms of two (filtered) images.

Given an image I and a filter F, the filtered image I_i can be recovered by $I_i = I*F$, where $*$ denotes a 2D convolution. Under the conditions as stated in [Sri02], the density functions of the filtered image I_i can be approximated by

$$f(x; p, c) = \frac{1}{Z(p,c)} |x|^{p-0.5} K_{(p-0.5)}\left(\sqrt{\frac{2}{c}} |x|\right) \tag{4}$$

where K the modified Bessel function and Z a normalization constant, given by

$$Z(p,c) = \sqrt{\pi}\Gamma(p)(2c)^{0.5p+0.25} \tag{5}$$

In order to estimate the required probability density functions, the parameters p and c have to be determined, based on the observed image pixel data, using

$$\hat{p} = \frac{3}{SK(I_i)-3} \text{ and } \hat{c} = \frac{SV(I_i)}{\hat{p}} \tag{6}$$

where SK represents the sample kurtosis and SV represents sample variance of the pixel values in I_i. Since the estimation of p is sensitive to the outliers, the estimation is replaced by an estimation based on quantiles, as proposed in [ZSC07]:

$$\widehat{SK}(I_i) = \frac{q_{0.995}(I_i) - q_{0.005}(I_i)}{q_{0.75}(I_i) - q_{0.25}(I_i)} \tag{7}$$

where $q_x(.)$ is the quantile function, that returns the x quantile of a set of samples. In order to analyze the performance on texture level, three images are selected: a synthetic finger-vein image, a real finger-vein image and a natural image. The images are scaled to the same size and the intensity values scaled to the same level. Thereafter a difference image between the original image and a 5 horizontal pixels shifted version is computed and Gabor filtered. Their estimated and observed pixel densities are comparatively illustrated figure 11. We selected 8 images from each of the three groups (real, synthetic, natural) and estimated their parameters as shown in table 6. The range of the estimated parameters from the real finger-vein images is quite similar or close to those from the synthesized finger-vein images. However these parameters are significantly different with those from the natural images.

In order to determine the differences between two Bessel K forms, different distance measures can be explored. The KL divergence [Sri02] between two density functions f_1 and f_2 is defined as follows:

$$d_{KL}(f_1||f_2) = \int_{IR} \log\left(\frac{f_1(x)}{f_2(x)}\right) f_1(x) dx \qquad (8)$$

The L^2-metric [Sri02] between two Bessel K can be computed as follows:

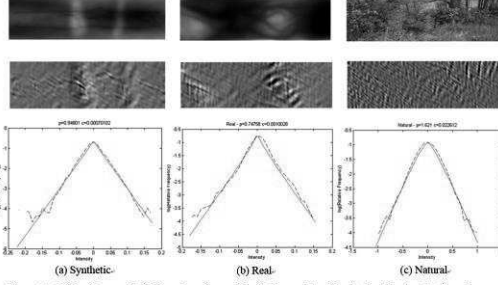$$d_I = \sqrt{\int_x \left(f(x; p_1, c_1) - f(x; p_2, c_2)\right)^2 dx} \qquad (9)$$

Table 1: Estimated Bessel K parameters for different images

Synthetic		Real		Natural	
p	c	p	c	p	c
1.10	5.85 10⁻⁴	1.13	4.36 10⁻⁴	3.86	0.062
0.81	4.67 10⁻⁴	1.21	5.85 10⁻⁴	0.60	0.11
1.03	5.56 10⁻⁴	1.73	1.49 10⁻⁴	1.62	0.023
1.04	5.01 10⁻⁴	0.75	0.0010	1.21	0.026
1.30	4.58 10⁻⁴	1.12	4.51 10⁻⁴	0.94	0.021
1.27	3.69 10⁻⁴	1.49	7.01 10⁻⁴	1.02	0.031
0.90	4.13 10⁻⁴	1.32	0.0017	1.32	0.024
1.08	5.00 10⁻⁴	1.25	6.44 10⁻⁴	2.14	0.22

Figure 11: Original images, their filtered versions and their observed densities (dashed lines) and estimaed Bessel K forms.

Using these distance measures, the Bessel K forms for the twelve images, four selected from each groups, *i.e.*, real, synthetic and natural, are compared and classified. All images were scaled/selected to be of same size where after the difference image is computed and Gabor filtered. Their Bessel K forms are estimated and compared, using the both distance measures in equation (8) and (9). The dendrogram plots in figure 12 illustrate the results of the classifications, based on these comparisons. In this figure, number 1-4 denote natural images, 5-8 denotes real finger-vein images and 9-12 denote synthetic finger-vein images. It can be observed that the natural images are distinctly classified from the finger-vein images in both the cases.
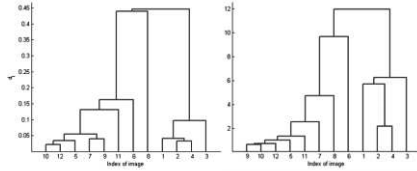

Figure 12: Dendrogram clustering of the distance metrics d_I (left) and d_{KL} (right). 1-4 natural, 5-8 real finger vein, while 9-12 are synthetic finger-vein images.
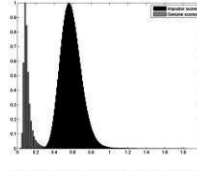
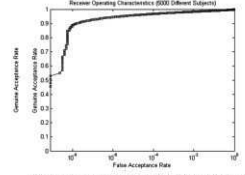Figure 13: Normalized histograms of the genuine and impostor matching scores

Figure 14: Receiver operating characteristics from synthetic finger-vein images.

6.3 Identification Performance

The key purpose of synthetic finger-vein generation is for the performance evaluation of biometrics recognition algorithms. The recovery of finger-vein images using anatomical characteristics and incorporating realistic imaging variations, such as from the model in this paper, can help to estimate upper bound [KK13] on the performance from the finger-vein matching technologies. We ascertain finger-vein matching performance from the database corresponding to 5000 subjects using their 50,000 synthesized finger-vein images. The matcher employed in our experiments is based on recovering and matching binary pattern (LBP). The synthetic images are firstly enhanced, using the histogram equalization. The normalized LBP histograms are then computed, using 8 subparts, a radius of 5 pixels and 8 sample points on this radius. The matching scores are computed

from the histogram similarity using the Chi squared distance [Gag10]. We generated 225000 genuine scores and 1249750000 impostor scores to estimate the matching accuracy for large scale database. The normalized histogram of these scores is shown in figure 13, while its receiver operating characteristics is shown in figure 14. The experiments achieve an equal error rate of 1.63%.

7 Conclusions and Further Work

This paper has presented a first attempt to model synthetic finger-vein generation and developed a synthetic finger-vein database of 50,000 images corresponding to 5000 different subjects. Our synthetic model is based on anatomical characteristics of fingers and incorporates realistic imaging variations introduced in the finger-vein imaging sensors. Our anaysis in section 6.2 suggests that the synthesized finger-vein images from the proposed model very closely follows (comparisons using Bessel K form) real finger-vein images acquired using conventional approaches. We also presented matching performance corresponding to 5000 different subjects, using 225,000 genuine and more than 1249 million impostor scores, which indicate significant potential from this modality for the large scale biometrics applications.

Despite first promising effort [HK14] towards synthesizing realistic finger-vein images detailed in this paper, there are several areas which need further work. In our work, we assumed relatively constant intra-class illumination for the same subjects/finger images. However during the real finger-vein imaging the variations in the illumination, especially for the same class images, can be much larger. Therefore further work is required to incoperate such expected variations in the imaging.

Acknowledgement

References

[BGTK06]   Alexey N. Bashkatov, Elina A. Genina, Vyacheslav I. Kochubey and Valery V. Tuchin. Optical properties of human cranial bone in the spectral range from 800 to 2000 nm. In *Saratov Full Meeting 2005: Optical Technologies in Biophysics and Medicine VII.* International Society for Optics and Photonics, 2006.

[BK10]   A. Buryanov and V. Kotiuk. Proportions of Hand Segments. *Int. J. Morphol,* 28(3):755-758, 2010.

[BV99]   Volker Blanz and Thomas Vetter. A morphable model for the synthesis of 3D faces. In *Proceedings of the 26th annual conference on Computer graphics and interactive techniques,* pages 187-194. ACM Press/Addison-Wesley Publishing Co., 1999.

[Cap04]   Raffaele Cappelli. SFinGe: an approach to synthetic fingerprint generation. In *International Workshop on Biometric Technologies (BT2004)*, pages 147-154, 2004.

[CC+07]   Septimiu Crisan, TE Crisan et al. A low cost vein detection system using near infrared radtiation. In *Sensors Applications Symposium, SAS'07.* 1-6. IEEE, 2007

[HK14]   Synthetic Finger Vein Image Database Generator, http://www.comp.polyu.edu.hk/~csajaykr/fvgen.htm, June 2014

[Gag10]   N.D. Gagunashvili. Chi-square tests for comparing weighted histograms. *Nuclear Instruments and Methods in Physics Research Section A: Accelerators, Spectrometers, Detectors and Associated Equipment* 614.2 (2010): 287-296

[Gra18]   Henry Gray. Anatomy of the human body, 1918.

[GS01]   Ulf Grenander and Anuj Srivastava. Probability models for clutter in natural images. *IEEE Transactions on Pattern Analysis and Machine Intelligence,* 23(4):424-429, 2001.

[KK13]   Ajay Kumar and Cyril Kwong, "Towards contactless, low cost and accurate 3D fingerprint identification," *Proc. CVPR 2013*, Portland, pp. 3438-3443, June 2013.

[KP07]   Byung Jun Kung and Kang Ryoung Park. Real-time image restoration for iris recognition systems. *IEEE Transactions on Systems, Man, and Cybernetics, Part B: Cybernetics,*37(6):1555-1566, 2007.

[KP09]   Ajay Kumar and K. V. Prathyusha. Personal authentication using hand vein triangulation, *Image Processing*, *IEEE Transactions on*, 38(9): 2127-2136, 2009

[KZ12]   Ajay Kumar and Yingbo Zhou. Human identification using finger images. *Image Processing, IEEE Transactions on,* 21(4):2228-2244, 2012.

[LLP09]   Eui Chul Lee, Hyeon Chang Lee, and Kang Ryoung Park. Finger-vein recognition using minutia-based alignment and local binary pattern-based feature extraction. *International Journal of Imaging Systems and Technology,* 19(3):179-186, 2009.

[Lod99]   Guillermo Loda. *Atlas of thumb and finger reconstruction.* Thieme, 1999.

[LP11]   Eui Chul Lee and Kang Ryoung Park. Image restoration of skin scattering and optical blurring for finger vein recognition. *Optics & Lasers in Engineering,* 49(7):816-828, 2011.

[MASR14]   Mohd Shahrimie, Mohd Asaari, Shahrel A. Suandi and Bakhtiar Affendi Rosdi. Fusion of band limited phase only correlation and width centroid contour distance for finger based biometrics. *Expert Systems with Applications,* 41(7):3367-3382, 2014.

[MNM04]   Naoto Miura, Akio Nagasaka and Takafumi Miyatake. Feature extraction of finger-vein patterns based on repeated line tracking and its application to personal identification. *Machine Vision and Applications,* 15(4):194-203, 2004.

[Per]   Ken Perlin. Noise and Turbulence. http://mrl.nyu.edu/~perlin/doc/oscar.html

[RFL⁺05]   Adam Runions, Martin Fuhrer, Brendan Lane, Pavol Federl, Anne-Gaëlle Rolland-Lagan and Przemyslaw Prusinkiewicz. Modeling and visualization of leaf venation patterns. In *ACM Transactions on Graphics (TOG),* 15: 702-711. 2005.

[RSS11]   Bakthiar Affendi Rosdi, CHai Wuh Shing and Shahrel Azmin Suandi. Finger vein recognition using local line binary pattern. *Sensors,* 11(12):11357-11371, 2011.

[SND⁺07]   A. Sukop, O. Naňka, M. Dušková, M. TVRdek, R. Kufa, O. Měšťák and L. Hauschwitcová. Clinical anatomy of the dorsal venous network in fingers with regards to replantation. *Clinical Anatomy,* 20:77-81, 2007.

[Sri02]   Anuj Srivastava. Stochastic models for capturing image variability. *Signal Processing Magazine, IEEE,* 19(5):63-76, 2002.

[TV13]   B. T. Ton and R. N. J. Veldhuis. A high quality finger vascular pattern dataset collected using a custom designed capturing device. In *Biometrics (ICB), 2013 International Conference on,* pages 1-5. 2013.

[WHST08]   Zhuoshi Wei, Yufei Han, Zhenan Sun and Tieniu Tan. Palmprint image synthesis: A preliminary study. In *Image Processing, 2008. ICIP 2008. 15ᵗʰ IEEE International Conference on,* pages 285-288, 2008.

[XS08]   Li Xueyan and Guo Shuxu. The fourth biometric – Vein recognition. *Pattern Recognition Techniques, Technology and Applications,* 626, 2008.

[YLS11]   Yilong Yin, Lili Liu and Xiwei Sun. SDUMLA-HMT: a multimodel biometric database. In *Biometric Recognition,* pages 260-268. Springer, 2011.

[YS12]   Jinfeng Yang and Yihua Shi. Finger-vein ROI localization and vein ridge enhancement. *Pattern Recognition Letters,* 33(12):1569-1579, 2012.

[YSY10]   Jinfeng Yang, Yihua Shi and Junli Yang. Finger-vein recognition based on a bank of Gabor filters. In *Computer Vision-ACCV 2009,* pages 374-383. Springer, 2010.

[YSY12]   Jinfeng Yang, Yihua Shi and Jucheng Yang. Finger-Vein image restoration based on a biological optical model. 2012.

[ZLL⁺13]   Congcong Zhang, Xiaomei Li, Zhi Liu, Qijun Zhao, Hui Xu and Fangqi Su. The CFVD reflection-type finger-vein image database with evaluation baseline. In *Biometric Recognition,* pages 282-287. Springer 2013.

[ZSC07]   Jinyu Zuo, Natalia A. Schmid and Xiaohan Chen. On generation and analysis of synthetic iris images. *Information Forensics and Security, IEEE Transactions on,* 2(1):77-90, 2007